Reprinted from
Journal of Imaging Science and Technology® 65(5): 050403-1–050403-15, 2021.

Development of a System to Measure the Optical Properties of Facial Skin using a 3D Camera and Projector

Kumiko Kikuchi▲
Shiseido Co., Ltd., MIRAI Technology Institute, 1-2-11 Takashima, Nishiku, Yokohama 220-0011, Japan
E-mail: kumiko.kikuchi1@shiseido.com

Shoji Tominaga▲
Department of Computer Science, Norwegian University of Science and Technology, 2815 Gjøvik, Norway
Department of Business and Informatics, Nagano University, Ueda 386-1298, Japan

Jon Y. Hardeberg▲
Department of Computer Science, Norwegian University of Science and Technology, 2815 Gjøvik, Norway

Abstract. *We have developed a system to measure both the optical properties of facial skin and the three-dimensional shape of the face. To measure the three-dimensional facial shape, our system uses a light-field camera to provide a focused image and a depth image simultaneously. The light source uses a projector that produces a high-frequency binary illumination pattern to separate the subsurface scattering and surface reflections from the facial skin. Using a dichromatic reflection model, the surface reflection image of the skin can be separated further into a specular reflection component and a diffuse reflection component. Verification using physically controlled objects showed that the separation of the optical properties by the system correlated with the subsurface scattering, specular reflection, or diffuse reflection characteristics of each object. The method presented here opens new possibilities in cosmetology and skin pharmacology for measurement of the skin's gloss and absorption kinetics and the pharmacodynamics of various external agents.*
[DOI: 10.2352/J.ImagingSci.Technol.2021.65.5.050403]

1. INTRODUCTION

Quantitative assessment of human skin for its visual qualities, including skin radiance, skin gloss and skin translucence, is a subject of great interest in the fields of dermatology, cosmetology and computer graphics.

These visual qualities of skin are related to the perceptual response to light reflected from the skin [1]. In addition, light that is reflected from the skin is the result of complex optical interactions between the light that is incident on the skin and the physical properties of the skin itself [2–4]. Therefore, accurate measurement of the physical properties of skin that affect its visual quality, i.e., the measurement of the skin's optical properties, is important. And by understanding its optical properties, we will be able to explain the visual qualities of skin.

When light from the external source is incident on the skin, part of the light is reflected from the skin's surface and the remainder penetrates the skin [5]. On the skin's surface, the presence of a thin emulsified film due to the presence of sebum affects specular reflection, in addition to the effects of contours derived from the shape of the face and the geometric heterogeneity of the surface roughness caused by pores, fine wrinkles and other irregularities [6]. Specular reflection affects the perception of the skin's radiance and gloss [3, 7].

Light that has entered the interior of the skin is reflected diffusely by the microstructure of the stratum corneum [8]. The stratum corneum is generally clear and colorless and there is usually little light absorption within this layer, thus allowing the light to continue and reach the deeper skin layers, including the epidermis, dermis and beneath. There, the light is absorbed by skin pigments, including melanin in the epidermis and hemoglobin in the dermis, and finally, some of the light then emits from the skin and comes back to the initial medium (air) in the form of subsurface scattering [1, 5].

This diffuse reflection and subsurface scattering behavior is believed to affect the perception of the "translucency" and the "dullness" of the skin [4, 8, 9].

Several methods have been proposed to separate and measure the optical properties of skin, including the specular reflection, diffuse reflection and subsurface scattering of the skin.

The main method used for separation and measurement of the skin specular reflection component involves use of two polarizing plates [6, 7, 10, 11]. The specular reflection does not retain the polarization characteristics of the incident light [12]. When the incident light is linearly polarized, there will be changes in the direction of vibration, although the light will be still linearly polarized. The polarized light by specular reflection does not transmit though the polarizing filters. The diffuse reflection component (D) can be acquired by arranging the polarizing filters at right angles to both

▲ IS&T Members.

Received June 4, 2021; accepted for publication Sept. 14, 2021; published online Oct. 12, 2021. Associate Editor: Markku Hauta-Kasari.
1062-3701/2021/65(5)/050403/15/$25.00

the light-emitting device and the light-receiving device. The specular reflection component (S) can then be measured independently by subtracting the amount of light for the diffuse reflection component from the total amount of light measured when the polarizing filters are arranged in parallel. However, strictly speaking, this method does not provide direct measurement of the light that passes through the inner skin layers.

In addition, several methods have been proposed to separate and measure the subsurface scattering from the skin. Examples include a method that observes the spread of the internal light by injecting either laser light or a slit light into the skin [13–15] and a method in which transmitted light is received at different distances from the incident light [9]. Additionally, methods have been proposed to express the distribution of the subsurface scattering from the skin in a two-dimensional image by scanning a projected grid pattern on the skin [16–18].

As mentioned earlier, there are many ways to acquire surface reflected light and subsurface scattering signals using independent devices. However, there are few examples of the development of systems that can acquire all optical properties that affect the skin texture on the face, in addition to acquisition of the geometry of the skin [14, 19, 20].

By obtaining the three-dimensional shape of the face and its optical properties simultaneously, it becomes possible to observe the captured facial images not only from the single direction of a two-dimensional image but also from various angles. Observing the face from various angles, just like observing the face in the real world, is effective in many industrial fields such as cosmetics development and computer graphics. In addition, it is also useful in sensory evaluation to evaluate the "skin's visual qualities". Therefore, it is expected to be used in various areas of basic research.

To measure the optical conditions of multiple skin types in the fields of dermatology and cosmetology and confirm the effects of cosmetics and external preparations on these different skin types, it is necessary to construct a system that takes a minimal time to perform measurements and requires few images for analysis. In addition, to measure the skin condition accurately, it is necessary to design the system to be as compact as possible to enable it to be transported to a temperature- and humidity-controlled room.

The present paper's focus is on the development of a system that can measure the geometrical shape and the optical properties of facial skin simultaneously and the data acquisition that can be used for reference in many areas of applied research, including confirmation of the effectiveness of cosmetics and exodermis. Our capture system was designed newly using a 3D camera and projector, although the basic measurement principles were based on the combination of these measurement techniques. It is novel to develop the acquisition system that obtains both the optical properties and the three-dimensional shape of facial skin. When these measurement data are available, we can render realistic 3D computer graphics of human face under different conditions of illumination and viewing. The rendered images should be closer to real human skin because the three essential components of diffuse reflection, specular reflection, and subsurface scattering are taken into account. This technology can be successfully applied in industrial fields such as cosmetics development and computer graphics.

2. DEVELOPMENT OF A SYSTEM TO MEASURE THE OPTICAL PROPERTIES OF FACIAL SKIN

2.1 *System Configuration*

We have developed a system to measure the optical properties of facial skin that consists of a light field camera and a lighting device, and have installed this system in a darkroom (Figure 1).

A light field camera (R-29; Raytrix GmbH, Kiel, Germany) was used because it is capable of 3D information acquisition. Normally, the image of a subject observed by the camera is focused within the depth of field of the main lens, and it is thus necessary to vary the focus of the main lens to change the focal plane and observe different focal images separately. In contrast, in a light field camera, microlenses with various focal lengths are placed over the entire surface of the camera's image sensor. A variety of focal images can then be acquired without varying the focus of the main lens and the 3D information can be reconstructed from the focal images acquired by each microlens [21]. The image sensor in the light field camera used in this study is a progressive scan-type charge-coupled device (CCD) with resolution of 6576×4384 pixels. A focused image and a depth image that includes distance information can be obtained from a single shot acquired using only one camera.

The focused image obtained from the light field camera is a red-green-blue (RGB) 16-bit Tag Image File Format (TIFF) image with an image size of 3288×2192 pixels. Fig. 1(c) shows the relative spectral sensitivity characteristics of the RGB channels of the light field camera used in the system. This plot shows the *RGB* values extracted from images acquired at each wavelength while irradiating a white plate (CS-A5; Konica Minolta, Inc., Japan) installed in the darkroom booth with equal-energy single-wavelength light using a programmable lighting system (ELS-VIS 800; Nikon Corp., Japan). We investigated whether the measured camera responsiveness obeys the Luther condition. [22] As a result of comparing the 2-deg *XYZ* color matching functions with the camera, the root mean squared error was $RMSE = 0.18725$, i.e., the camera responsivities do not completely obey the Luther condition (Fig. 1(d)). In this study, limited to the skin color gamut, we assumed linearity for *RGB* and *XYZ* values and modeled by empirical rule.

The accuracy of the depth image acquired from the light field camera is dependent on both the focused image structure and the local contrast. The focused image can be combined with the distance information to reconstruct the 3D surface.

A single-chip digital light processing projector (PJ WXC1110; Ricoh Co., Ltd., Japan) was used as the lighting device. The light source for this projector is an *RGB* light-emitting diode and its resolution is 1280×800 pixels

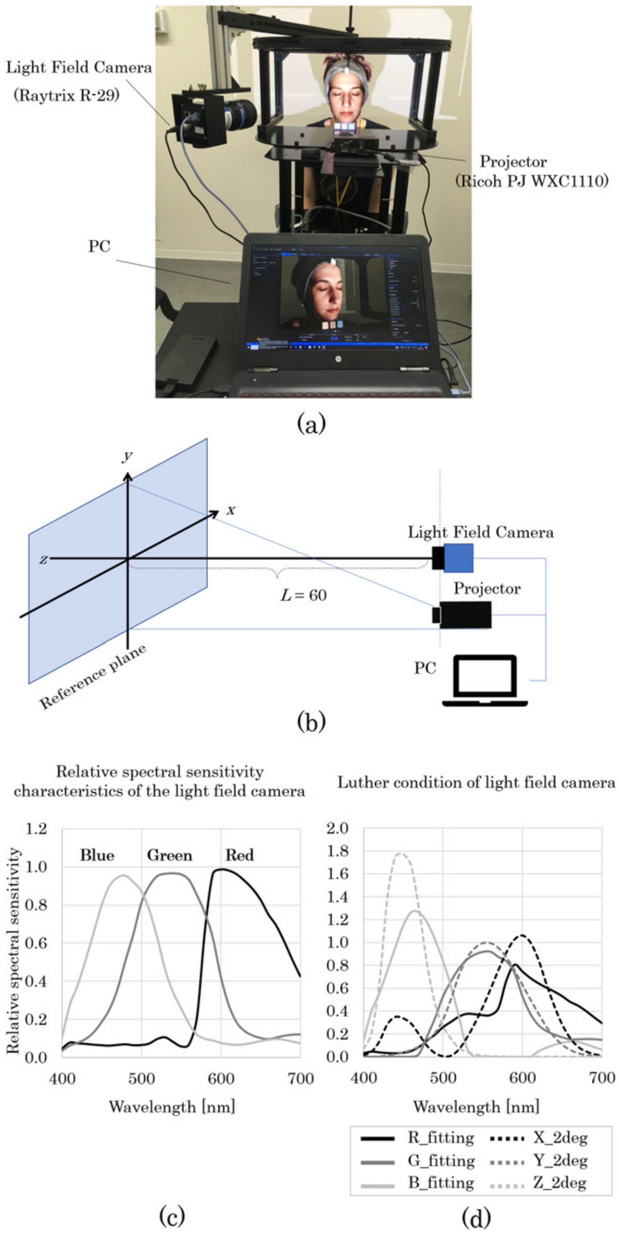

Figure 1. (a) Front view photograph of the system. The system is installed in a darkroom. (b) Schematic of the system. (c) Relative spectral sensitivity characteristics of the light field camera. (d) Quality evaluation for the filters of light field camera.

(Wide Extended Graphics Array or WXGA standard). This projector provides sufficient irradiance to acquire both 3D and color information from a subject's face and can also generate various lighting patterns to separate the subsurface scattering from the surface reflection from the facial skin. Figure 2 shows the spectral radiance characteristics of the *RGB* primaries of the projector. The CIE-xy coordinates of the *RGB* primaries of the projector were Red = (0.6405, 0.3181), Green = (0.2825, 0.5905), Blue = (0.1619, 0.0759) for the color gamut of the projector on a Commission Internationale de l'Éclairage CIE-xy chromaticity diagram. These data were obtained by projecting the light from the projector onto the white plate installed in the darkroom booth and then measuring the white plate using a spectroradiometer (CS-2000A; Konica Minolta, Inc., Japan).

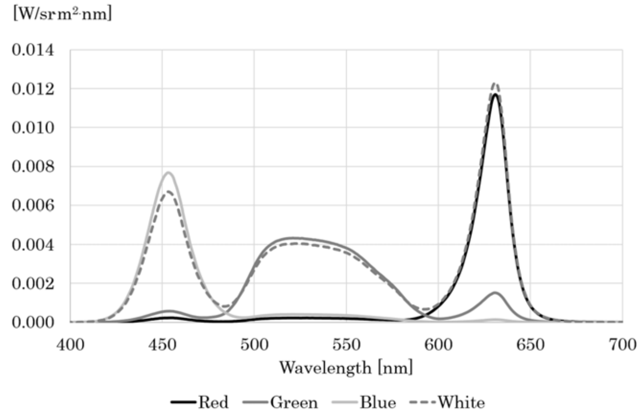

Figure 2. Spectral radiance characteristics of the *RGB* primaries and the white light of the projector.

2.2 *Color Calibration*

Images acquired using a normal camera are composed of *R*, *G*, and *B* channels and the output characteristics of these channels vary depending on the camera's spectral sensitivities. To calculate the CIE *XYZ* (CIE 1931 *XYZ* space) value and each index of the CIE $L^*a^*b^*$ (1976 CIELAB space) from the captured image, it is necessary to understand that the *RGB* output characteristics differ depending on the camera used and then construct an algorithm that converts the *RGB* output into an absolute reference value (e.g., the CIE *XYZ* value). Using the following three steps, we pre-built a conversion formula that can calculate the CIE XYZ_{D65} value from the *RGB* output of the light field camera's focused image (Figure 3). In this work, the 145 skin color chips (Skin Tone Color; Japan Color Research Institute, Japan) shown in Fig. 3 were used and the measurements were performed to obtain the CIE XYZ_{D65} values with a spectrophotometer (CM-700d; Konica Minolta, Inc., Japan).

Step 1: Select the color chips contained within the skin color area and measure the CIE XYZ_{D65} values of these color chips.

Step 2: Set all pixels of the projector, which is the lighting component of the system, to white light (*RGB* = (255, 255, 255)), illuminate the color chart, and image with the light field camera to acquire the *RGB* values of the color chart areas in the focused images.

Step 3: Perform multiple regression analysis using the XYZ_{D65} values of the color chips acquired in Step 1 as the objective variables and the*RGB* values of the color chips acquired in Step 2 as the explanatory variables to obtain the conversion formula that can calculate the reference value XYZ_{D65} from the *RGB* values of the camera output.

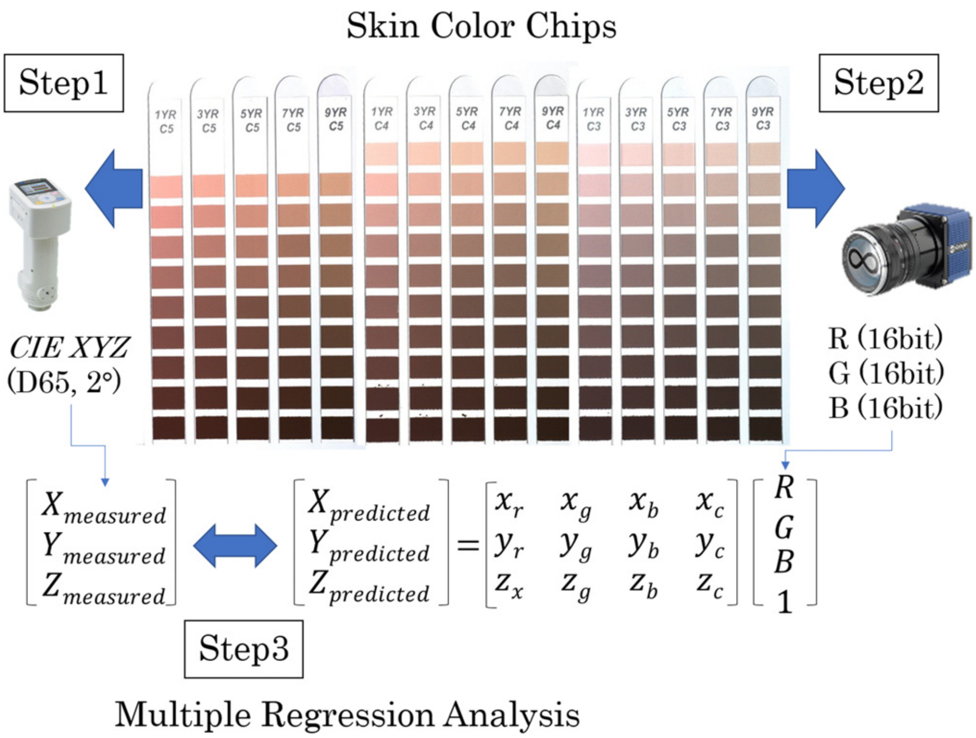

Figure 3. Steps performed to calculate the CIE XYZ_{D65} values from the RGB output of the light field camera.

The conversion formula obtained from this procedure is shown as Eq. (1)

$$\begin{bmatrix} X \\ Y \\ Z \end{bmatrix} = \begin{bmatrix} 3.064 \times 10^4 & 0.721 \times 10^4 & 5.526 \times 10^4 & 1.123 \\ 0.825 \times 10^5 & 6.020 \times 10^4 & 3.086 \times 10^4 & 1.149 \\ -7.875 \times 10^5 & -5.404 \times 10^4 & 1.550 \times 10^3 & 0.490 \end{bmatrix} \begin{bmatrix} R \\ G \\ B \\ 1 \end{bmatrix}. \tag{1}$$

Equation (2) shows the procedure used to derive each index of the CIE $L^*a^*b^*$ (1976 CIELAB space) from the CIE XYZ_{D65}.

$$L^* = 116 \times f\,(Y/Y_w) - 16$$
$$a^* = 500 \times \left[f\,(X/X_w) - f\,(Y/Y_w)\right]$$
$$b^* = 200 \times \left[f\,(Y/Y_w) - f\,(Z/Z_w)\right],$$

where

$$f\,(t) \begin{cases} t^{1/3} & t > (6/29)^3 = 0.008856 \\ \left[(29/3)^3\, t - 16\right]/116 & t \leq (6/29)^3 = 0.008856 \end{cases}$$

Under D65 illuminant conditions,

$$X_w = 95.039, \quad Y_w = 100, \quad Z_w = 108.88. \tag{2}$$

Figure 4(a) shows the correlation between the measured XYZ_{D65} values of the color chips obtained using the spectrophotometer and the XYZ_{D65} values predicted when Eq. (1) is applied to the camera output. Fig. 4(b) shows the correlation between the measured $L^*a^*b^*$ values of the color chips and the predicted $L^*a^*b^*$ values from the camera that were obtained using Eqs. (1) and (2). The average color difference (ΔE_{ab}) between the value measured using the spectrophotometer and the value predicted by this system was 1.445 for the 145 color chips. The maximum color difference was 2.324, and the minimum color difference was 0.2723. The maximum color difference occurred in the color chip of $HVC = (1YR, 8.0, 5.0)$, which was the most reddish color among the color chips used to create the conversion formula (i.e., the boundary of the skin color range). When the color chip with the maximum color difference was excluded, the average color difference was 1.399.

3. ACQUISITION OF SKIN OPTICAL PROPERTY PARAMETERS

3.1 *Outline*

The light that irradiates the skin is divided into the proportion of the light that is reflected from the surface of the skin and the proportion of the light that is transmitted through the interior of the skin [5]. The light reflected from the surface of the skin is specular reflection, which is reflected

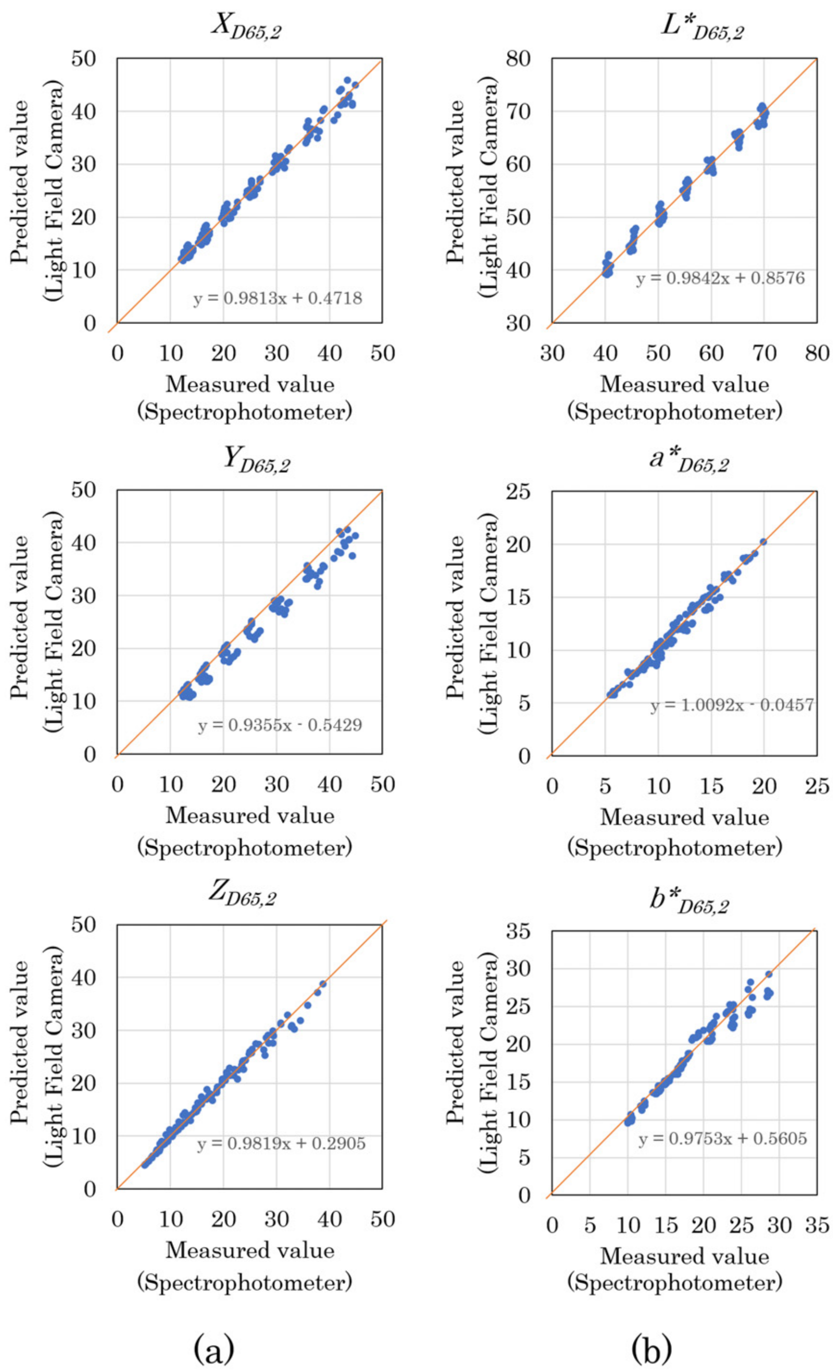

Figure 4. Comparison of the measured value of the color sheet with the predicted value calculated from the camera output. (a) Correlation between the measured XYZ_{D65} values of the color chips obtained using the spectrophotometer and the predicted XYZ_{D65} values obtained from the camera. (b) Correlation between the measured $L^*a^*b^*$ values of the color chips and the predicted $L^*a^*b^*$ values obtained from the camera.

with a strength that depends on the angle of incidence of the light (Figure 5(a)).

The light reflected from a layer located very close to the surface is diffuse reflection, which is diffused in all directions (Fig. 5(b)).

The proportion of the light that penetrates the skin is affected by absorption by melanin in the epidermis and by hemoglobin in the capillaries of the dermis. In addition, the light is affected by scattering in each layer, which causes it to spread in various directions, and it then exits the skin from points other than the incident point (subsurface scattering; Fig. 5(c)). As will be described later, our system acquires light that has exited with a propagation distance of 1.0 mm or more in the skin as the subsurface scattering component.

In this study, the subsurface scattering component (Fig. 5(c)) is first separated from the light reflected from the skin. The surface reflection component is then obtained by subtracting this subsurface scattering component from the

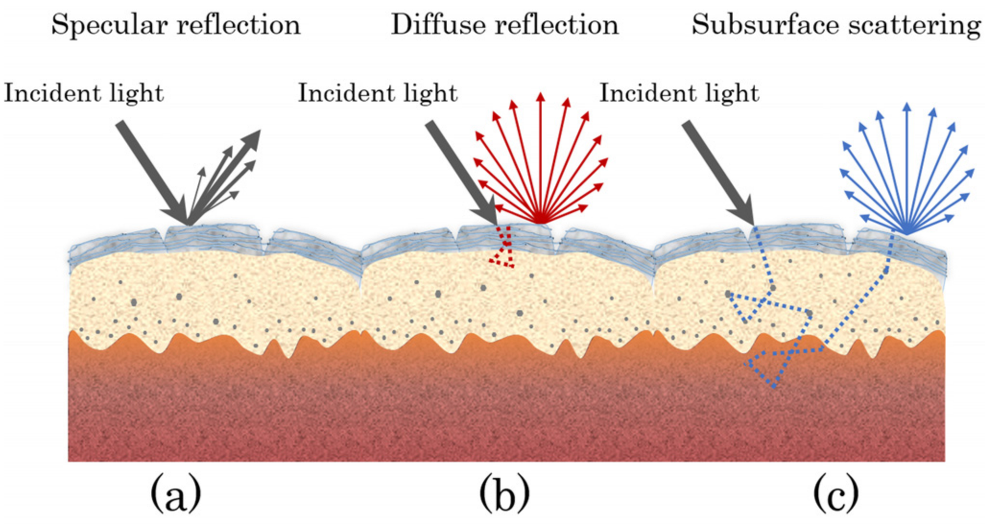

Figure 5. (a) Specular reflection from the skin surface. (b) Diffuse reflection. (c) Subsurface scattering.

total amount of light that is reflected from the skin. The surface reflection component in this case includes both the diffuse reflection component (Fig. 5(b)) and the specular reflection component (Fig. 5(a)). The diffuse reflection component is then calculated by applying the dichromatic reflection model to the surface reflection component. Finally, the specular reflection component is acquired by subtracting the diffuse reflection component from the surface reflection component.

3.2 *Separation of the Subsurface Scattering Component*

In this study, we use the theory proposed by Kuwahara [15] and a calculation method based on high-frequency illumination that was proposed by Nayar et al. [16] to separate the total light that is reflected from one point on the skin into the surface reflection and subsurface scattering components. The projector placed in front of the subject's face generates white light illumination, in which all the pixels of the projector are emitting white light, and binary square wave illumination, which is composed of vertical stripes produced by repeating four white pixels and four black pixels. When the skin is illuminated with the binary square wave illumination in a darkroom, the light that exits from the illuminated point (corresponding to the white pixels of the projector) has both a surface reflection component and a subsurface scattering component; however, only the subsurface scattering component then exits from the unilluminated point (corresponding to the black pixels of the projector). In our system, 4 pixels on the projector is equivalent to 1.0 mm on the skin. This means that the subsurface scattering light that has a propagation distance of 1.0 mm or more, exits at the unilluminated points. By projecting the high-frequency illumination while shifting it in the horizontal direction, each point on the skin surface changes to either the illuminated state or the unilluminated state. Using this relationship between the illuminated and unilluminated states, a calculation method that separates the direct component (corresponding to the surface reflection component of the skin in our system) and the global component (corresponding to the subsurface scattering component of the skin in our system) of the scene has been proposed [16]. At each point, a maximum value ($i_{\max}$) and a minimum value ($i_{\min}$) are obtained from the brightness values for the same pixel in a set of patterned light projection images. In this case, $i_{\max}$ indicates the brightness value when the point is illuminated and $i_{\min}$ indicates the corresponding value when that point is not illuminated.

On the other hand, the total brightness value observed at each point is the sum of the surface reflection component and the subsurface scattering component.

$$L = L_r + L_s, \tag{3}$$

where L_r indicates the surface reflection component, consisting of specular reflection and diffuse reflection, and L_s indicates the subsurface scattering component.

The analysis results by Nayar et al. [16] suggest the relationships of $i_{\max} = L_r + L_s/2$ and $i_{\min} = L_s/2$.

Therefore, the surface reflection component and the subsurface scattering component can be obtained from the pixel values at two projections as follows:

$$L_r = i_{\max} - i_{\min} \tag{4}$$

$$L_s = 2i_{\min}. \tag{5}$$

We used a white plate with perfect diffuse reflection properties to correct the image. The white plate was captured by the system before all calculations were performed. For all images captured by the system, the brightness value of the entire image was corrected so that the brightness value at the unilluminated points on the white plate is consistent with 0, that is, $i_{\min} = 0$ on the perfect reflecting diffuser.

By taking an image set acquired by shifting the high-frequency illumination, extracting the maximum and minimum brightness values at the same coordinates for each

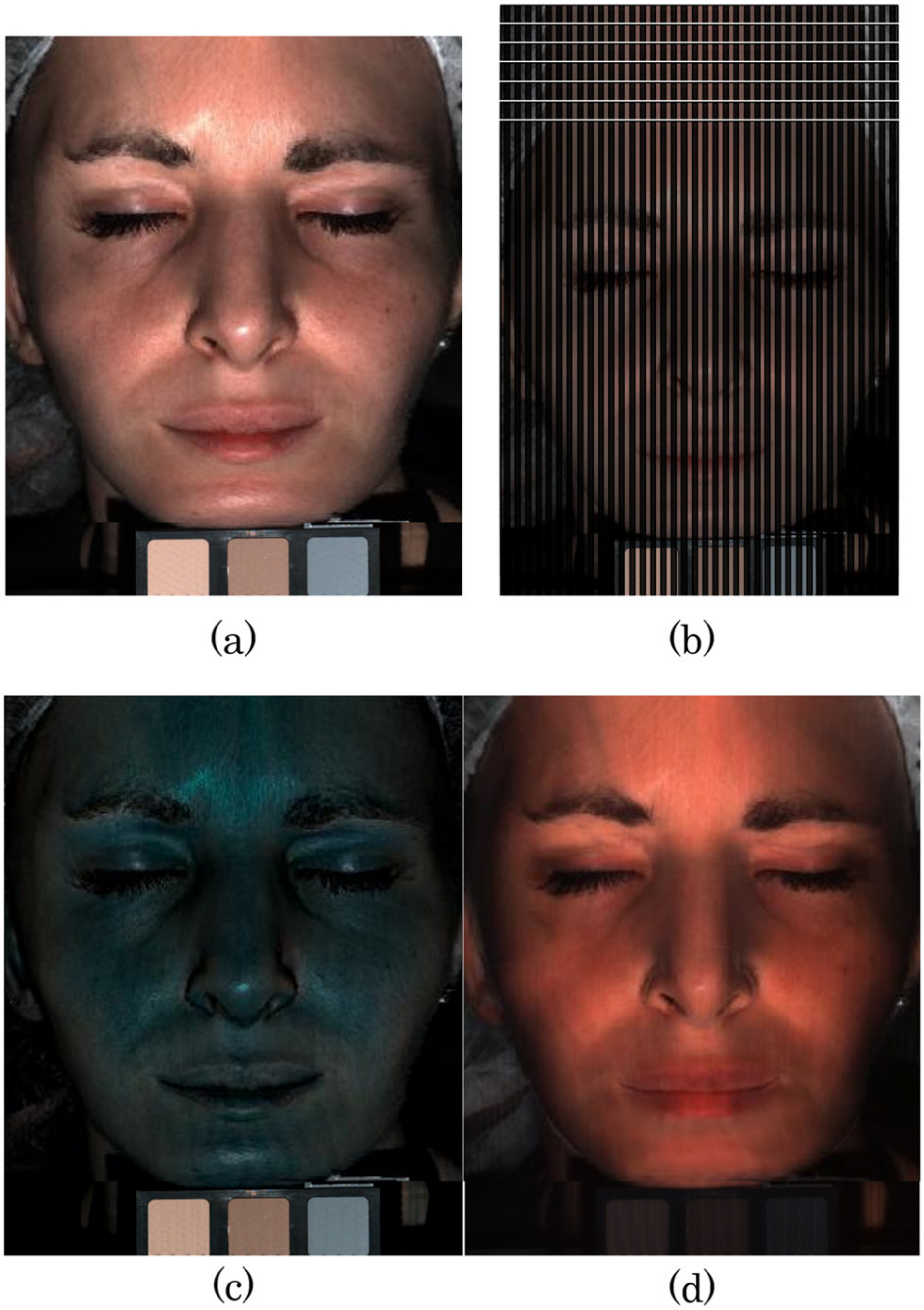

Figure 6. Separation of surface reflection component from subsurface scattering component using binary square wave illumination. (a) Focused image from light field camera. (b) Images acquired while shifting the binary square wave illumination. (c) Surface reflection component of the image. (d) Subsurface scattering component of the image. In this paper, the output value of the subsurface scattering component image from each RGB channel is multiplied by 1.5 and displayed for easy visual confirmation.

RGB channel, and executing the operations given by Eqs. (4) and (5), it becomes possible to generate images in which the surface reflectance component and the subsurface scattering component have been separated.

In the case of the binary square wave illumination in our system, one cycle consists of 8 pixels. By shifting the binary square wave illumination by 1 pixel in the horizontal direction, a set of eight images corresponds to one cycle. We acquired four cycles, i.e., a total of 32 images, to reduce the noise and the subsurface scattering component image (Figure 6(c) and (d), respectively).

By applying Eq. (1) to the *RGB* values of both the surface reflection component image and the subsurface scattering component image, respectively, the distribution image of the luminance Y for each light component with respect to the total appearance was generated.

3.3 *Separation of the Specular Reflection Components using the Dichromatic Reflection Model*

Several methods have been proposed for separation of the specular reflection components of the skin. In addition to use of a polarizing plate, there are methods that involve changing the direction of the light source [23] or moving the camera rather than moving the light source [24] to separate the specular reflection components. These methods require multiple images, but because this study is intended to measure the properties of facial skin, it is necessary to reduce the required measurement time to a minimum. Therefore, our system uses a separation method based on a dichromatic reflection model and generates an image in which only the diffuse reflection component is left from a single image acquired via the camera. The dichromatic reflection model proposed by Shafer states that the spectrum of the reflected light can be represented by a linear sum of the spectra of the specular reflection component and the diffuse reflection component [25]. In other words, when the reflected light has a brightness I, the brightness of the specular reflection component is I_s and the brightness of the diffuse reflection component is I_d, the relationship between these components can be expressed using a linear sum, as follows.

$$I = I_s + I_d. \tag{6}$$

In this paper, the specular and diffuse reflection components are separated using the following procedure based on a methodology [26] that uses the fact that the object follows the dichroic reflection model.

Step 1: Calculate the hue, saturation, and intensity in the hue-saturation-value (HSV) color space from the *RGB* values of each pixel in the surface reflection component image.

Step 2: Classify the pixels according to their hue values and plot the value of each pixel for which the hue value is constant on the saturation-intensity plane. On the saturation-intensity plane, the pixels that contain the specular reflection component have high intensity values and the pixels that contain the diffuse reflection component only have low intensity values in the iso-saturation region.

Step 3: Calculate the slope A of the straight line on which the pixels with diffuse reflection components only are plotted for each classified hue value.

Step 4: By recalculating the intensity values using slope A and the saturation values, it is then possible to obtain the diffuse reflection component with the specular reflection component removed at each pixel.

Step 5: Calculate the *RGB* value from the HSV value of each pixel in the obtained diffuse reflection component image by the inverse transformation of Step 1.

Specifically, in Step 2, the pixels that contain the diffuse reflection component only can be extracted by selecting the minimum intensity value for each saturation value, as shown in Figure 7. In Step 3, the intensity of the diffuse reflection component can be determined from the saturation values for all pixels by obtaining the slope A of a straight line using the least squares method. By subtracting the constructed diffuse reflection component image in Step 5 from the surface reflection component image, it is then possible to calculate an image of the specular reflection component alone (Figure 8). By applying Eq. (1) to the *RGB* values of both the diffuse reflection component image and the specular reflection component image, the distribution image of the luminance Y of each light component with respect to the total appearance was also generated.

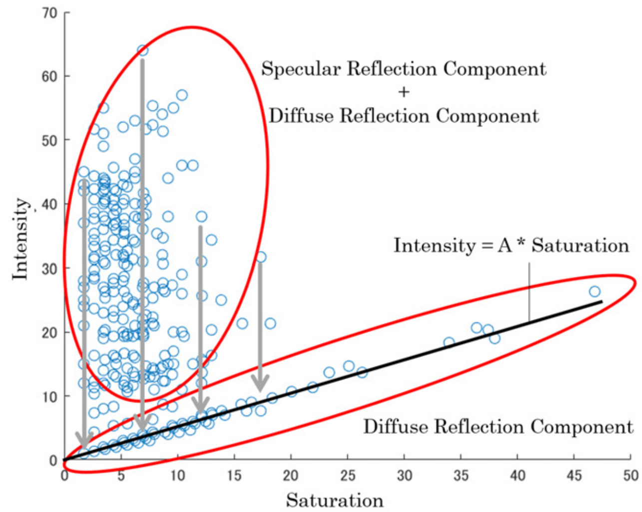

Figure 7. Separation of diffuse reflection component from specular reflection component using the dichromatic reflection model. Plane with saturation and intensity values plotted for pixels with the same hue. The pixels that contain the specular reflection component have high intensity values and the pixels that contain only the diffuse reflection component have low intensity values in the iso-saturation region. The intensity of the diffuse reflection component can be determined from the saturation values and the slope A of a straight line.

4. VERIFICATION OF SEPARATION ACCURACY OF OPTICAL PROPERTIES BY THE SYSTEM

4.1 *Confirmation of the Separation Accuracy of Optical Properties using Different Materials*

We used four different materials with different optical characteristics to confirm the accuracy of separation of material optical properties by the developed system. The four materials selected were fruit (an orange), metal (coins), pottery, and skin. Fruits provide both subsurface scattering and diffuse reflection in a manner similar to human skin. In addition, specular reflections can occur on both fruit and human skin, depending on the relationships between the object position, the lighting, and the camera. Metals do not produce subsurface scattering and offer only specular reflection. For the item of pottery, we selected a sample that was opaque and that did not have a smooth surface. Therefore, the pottery article only shows diffuse

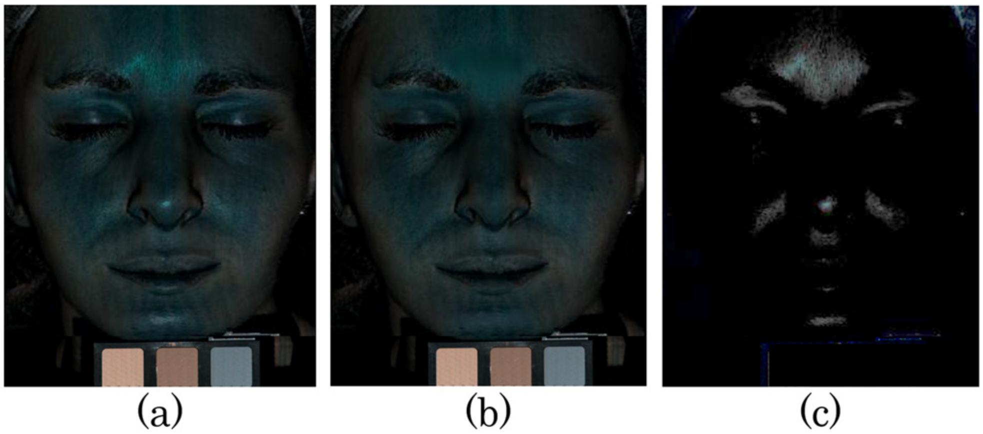

Figure 8. Results of separation of the diffuse reflection component and the specular reflection component using the dichromatic reflection model. (a) Surface reflection component. (b) Diffuse reflection component. (c) Specular reflection component.

reflection. These objects were placed in the system and their images were captured to enable separation of the subsurface scattering and surface reflection components. Through comparison of the characteristics of the separated images of the optical characteristics acquired by measuring these materials, we can qualitatively confirm the accuracy of separation of the optical characteristics by the system.

4.2 *Confirmation of the Separation Accuracy of Subsurface Scattering Components using Resin Objects*

We used a collection of resin objects created by Thomas et al. [27] to confirm the accuracy of separation of the subsurface scattering by the developed system. These objects, which varied in terms of their shapes, the ratios of their mixed material components, and their surface textures, and which also varied in a reasonably controlled manner, were made from Gédéo resin produced by Pébéo [28]. We selected five rectangular objects from the collection that had the same level of surface texture but different opacities. Each rectangular shape was created with dimensions of $27 \times 27 \times 15$ mm^3. The level of surface coarseness selected was the least smooth condition, which was defined as C3. The opacity was created by adding drops of white paint (Laquée semi-opaque, Pébéo Céramic) to the crystal resin. A white opaque resin was created by using 40 drops of white painting per 60 mL of the crystal resin. To produce the opacity range from transparent to white, the numbers of drops of white paint added to the crystal resin were 0 drops, 5 drops to 240 mL, 5 drops to 180 mL, 10 drops to 60 mL, and 40 drops to 60 mL. When these numbers were converted into the number of drops per mL, they were 0.000 drops/mL, 0.021 drops/mL, 0.028 drops/mL, 0.167 drops/mL, and 0.667 drops/mL, respectively. Each object was placed into the system and photographed to separate its subsurface scattering and surface reflection components.

5. SKIN MEASUREMENTS

Skin measurement tests were conducted in November 2019. The subjects were 150 Japanese women aged from their 20s to their 70s that lived in the Tokyo area. After washing the face and allowing the skin to acclimatize for 15 min, the skin was measured using the proposed system. We took precautions to prevent the light from the projector from shining directly into the eyes of each subject when acquiring the images. This study was approved by the Ethics Committee of the Shiseido Global Innovation Center. Informed consent was obtained from all participants. Table I lists the detailed parameters of the measurement environment.

Table I. Measurement dates and environment.

Measurement date	2019/10/17, 18, 19, 22, 23, 24
Average outdoor temperature (°C)	17.51±1.12
Average outdoor humidity (%)	71.17±5.84
Laboratory temperature (°C)	23
Laboratory humidity (%)	45

6. RESULTS

6.1 *Accuracy of Separation of the Optical Properties by the System*

Figure 9 shows the accuracy of separation of the optical properties of materials by the developed system. The individual parts of the figure show: (a) a focused image of four different materials, each with different optical characteristics, acquired under white light illumination from the projector; (b) a subsurface scattering component image calculated via projection of high-frequency patterned light; (c) a surface reflection component image, which was also calculated via projection of high-frequency patterned light; (d) a diffuse reflection component image that was calculated using the dichromatic reflection model; and (e) a specular reflection component image that was calculated by subtracting the diffuse reflection component image from the surface reflection component image. The subsurface scattering component image showed that strong surface scattering component levels were present on the skin and

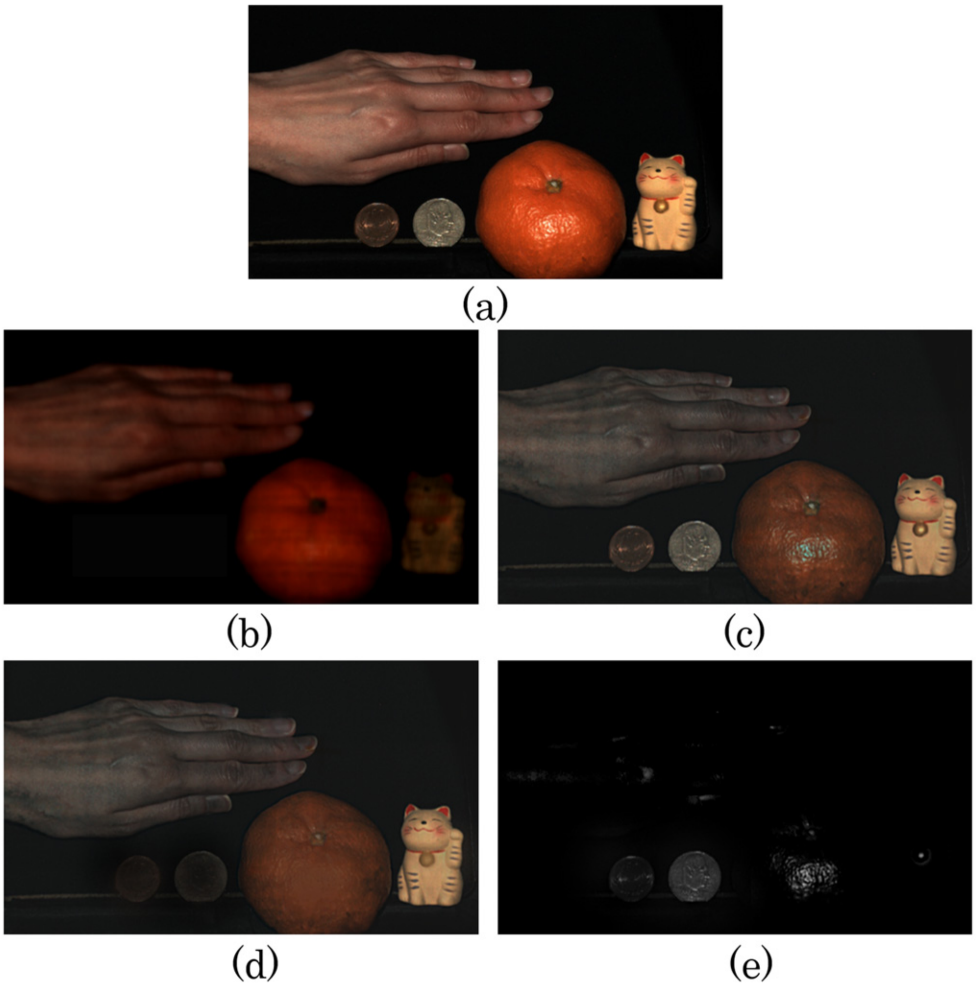

Figure 9. Accuracy of separation of material optical properties by the system. (a) Focused image of four different materials with different optical characteristics acquired under white light illumination from the projector. (b) Subsurface scattering component image calculated via projection of high-frequency patterned light. (c) Surface reflection component image calculated via projection of high-frequency patterned light. (d) Diffuse reflection component image calculated using the dichromatic reflection model. (e) Specular reflection component image calculated by subtracting the diffuse reflection component image from the surface reflection component image.

the fruit. In contrast, it was confirmed that no subsurface scattering components were observed in the metals. In addition, almost no subsurface scattering components were observed from the pottery. The diffuse reflection component image showed that diffuse reflection components were present on the skin, the fruit, and the pottery. The specular reflection component image showed that strong specular reflection was observed from the metals and from part of the fruit. There was also slight specular reflection from parts of the skin (the nail and the back of the hand) and from part of the pottery. From these results, we conclude that the separation of the material optical properties by the system can be correlated with the subsurface scattering, specular reflection, or diffuse reflection characteristics of each object.

6.2 *Accuracy of Determination of the Subsurface Scattering and Surface Reflection Components using Resin Objects*

Figure 10(a) shows focused images of five resin objects with different opacity levels that were acquired under white light illumination from the projector, the corresponding subsurface scattering component images calculated via projection of high-frequency patterned light, and the corresponding surface reflection component images, respectively. These images confirm that the level of the subsurface scattering component increases as the proportion of the white paint contained in the object increases. In contrast, the level of the surface reflection component seems to remain constant, regardless of the white paint content of the object. Fig. 10(b) shows the intensity values calculated from the *RGB* values over the area of each object captured from each component image. We constructed a method for calculation of the luminance values from the *RGB* values for colors in the skin color gamut, but because the resin objects have colors that lie outside the skin color gamut, we calculated their HSV values from the *RGB* values and then used their *V* values as their intensity parameters. As a result, it was confirmed that the intensity of the subsurface scattering component increased as the proportion of white paint contained in each object

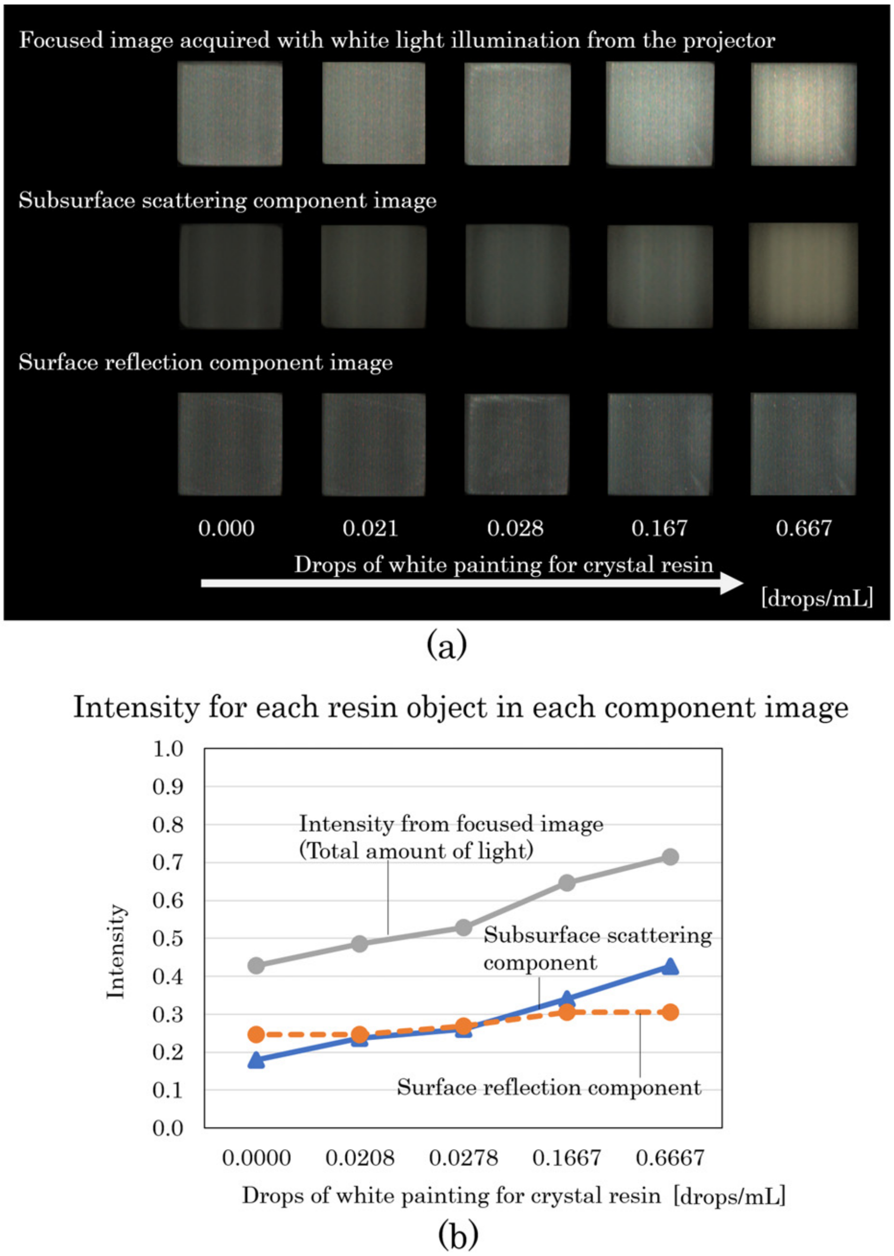

Figure 10. Subsurface scattering and surface reflection components of resin objects. (a) Focused image of five resin objects with different opacity levels acquired under white light illumination from the projector. (b) Subsurface scattering component image calculated via projection of high-frequency patterned light. (c) Surface reflection component image calculated via projection of high-frequency patterned light. (d) Intensity for each resin object in each component image.

increased. In contrast, the intensity of the surface reflection component remained constant, regardless of the proportion of white paint contained in the objects. From these results, we conclude that the separation of the subsurface scattering components provided by the system is correlated with the interior physical indicators of the materials.

6.3 *Features of each Light Component Image of Face*

Figures 11–13 show examples of the various skin measurements performed using this system. Fig. 11 shows an example of the optical characteristics of the skin of one woman in her twenties, Fig. 12 shows the corresponding characteristics of one woman in her forties, and Figure 13 shows the same characteristics of one woman in her sixties. To protect the personal information of the subjects, only the optical characteristics of each target subject's skin were morphed onto an average face created from the facial images of four subjects in each age group. Each section in figure 11 shows: (a) a focused image acquired under white light illumination from the projector; (b) the subsurface scattering component image calculated via projection of the high-frequency patterned light; (c) the surface reflection component image calculated via projection of the high-frequency patterned light; (d) the diffuse reflection component image calculated using the dichromatic reflection model; (e) the specular reflection component image calculated by subtracting the diffuse reflection component image from the surface reflection component image; and (f) an image that includes the diffuse reflection component and the subsurface scattering component; (g) an average shape created from the shapes of four subjects in each age group. Each three-dimensional image was reconstructed from the focused image and the distance information. Only the viewpoint was changed and the image is displayed as a two-dimensional image here; (h) a three-dimensional image reconstructed from the focused image and the distance information. Only the color data of each subject's skin were morphed onto the average shape in (g) created from the shapes of four subjects in each age group. The light source and its position were not varied–only the viewpoint was changed and the image is displayed as a two-dimensional image here.

Comparison of the subsurface scattering component image in (b) with the surface reflection component image in (c) shows that the subsurface scattering component image is generally reddish, but the surface reflectance component image is generally bluish. This result reflects the phenomenon that longer-wavelength light propagates more easily inside the skin than shorter-wavelength light.

Comparison of the diffuse reflection component image in (d) and the specular reflection component image in (e) shows that the diffuse reflection component image is a smooth image that lacks high-frequency information, whereas the specular reflection component image contains fine textures. This is because the specular reflection component is the light component that is reflected from the skin's surface and is thus affected by the unevenness of the skin's surface due to pores and fine wrinkles. In addition, it can be confirmed from these images that strong specular reflection occurs from the forehead and from the tip of the nose.

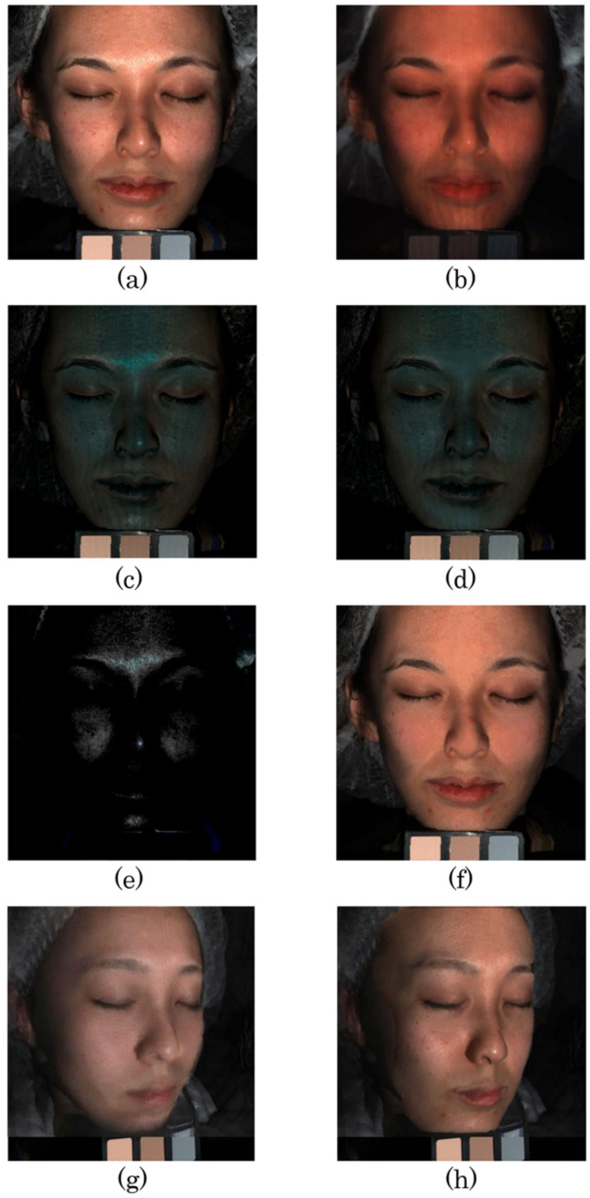

Figure 11. Separation of the optical properties of the skin of subject A, aged in her 20s. (a) Focused image acquired with white light illumination from the projector. (b) Subsurface scattering component image calculated through projection of the high-frequency patterned light. The output value from each RGB channel of the subsurface scattering component image was multiplied by 1.5 and then displayed for easy visual confirmation. (c) Surface reflection component image calculated through projection of the high-frequency patterned light. (d) Diffuse reflection component image calculated using the dichromatic reflection model. (e) Specular reflection component image calculated by subtracting the diffuse reflection component in (d) from the surface reflection component in (c). (f) Image including the diffuse reflection component in (d) and the subsurface scattering component in (b). (g) Average shape created from the shapes of four subjects aged in their 20s. Each 3D image was reconstructed from the focused image and the distance information. Only the viewpoint was changed and the image is displayed as a two-dimensional image here. (h) 3D image reconstructed from the focused image and the distance information. Only the color data of subject A's skin was morphed onto the average shape in (g). The light source and its position were not varied – only the viewpoint was changed and the image is displayed as a two-dimensional image here.

7. DISCUSSION

In this work, we have developed a measurement system that divides the light that is reflected from facial skin into the subsurface scattering component, the diffuse reflection component and the specular reflection component, and also acquires the three-dimensional shape of the subject's face.

Although there are some ways to acquire surface reflected light and subsurface scattering signals using independent devices, there are few examples of the development of systems that can acquire all optical properties that affect the skin texture on the face, in addition to acquisition of the geometry of the skin. By obtaining the three-dimensional shape of the face and its optical properties simultaneously, it becomes possible to observe the captured facial images not only from the single direction of a two-dimensional image, but also from various angles. Observing the face from various angles, just like observing the face in the real world, is useful in many industrial fields such as cosmetics development and computer graphics. In addition, it is also useful in sensory

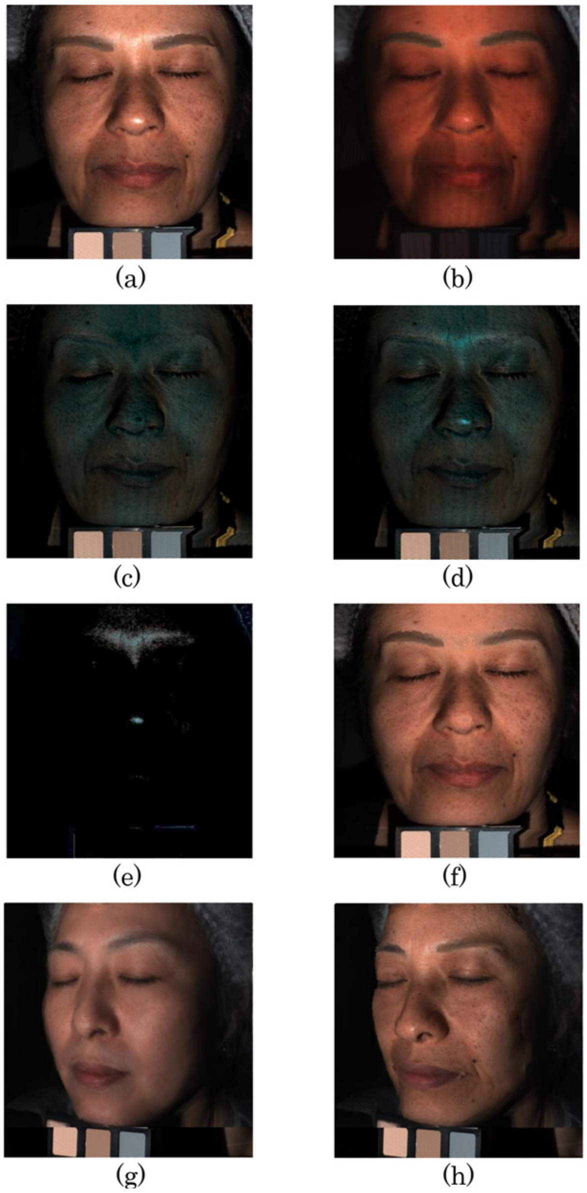

Figure 12. Separation of the optical properties of the skin of subject B, aged in her 40s. (a) Focused image acquired with white light illumination from the projector. (b) Subsurface scattering component image calculated through projection of the high-frequency patterned light. The output value from each RGB channel of the subsurface scattering component image was multiplied by 1.5 and then displayed for easy visual confirmation. (c) Surface reflection component image calculated through projection of the high-frequency patterned light. (d) Diffuse reflection component image calculated using the dichromatic reflection model. (e) Specular reflection component image calculated by subtracting the diffuse reflection component in (d) from the surface reflection component in (c). (f) Image including the diffuse reflection component in (d) and the subsurface scattering component in (b). (g) Average shape created from the shapes of four subjects aged in their 40s. Each 3D image was reconstructed from the focused image and the distance information. Only the viewpoint was changed and the image is displayed as a two-dimensional image here. (h) 3D image reconstructed from the focused image and the distance information. Only the color data of subject B's skin was morphed onto the average shape in (g). The light source and its position were not varied – only the viewpoint was changed and the image is displayed as a two-dimensional image here.

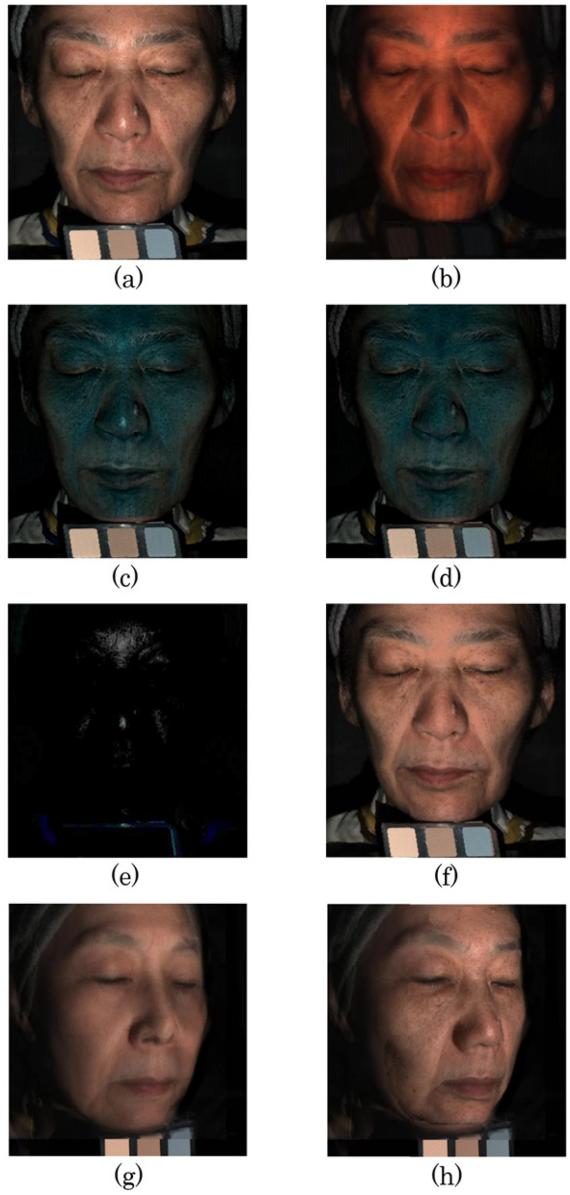

Figure 13. Separation of the optical properties of the skin of subject C, aged in her 60s. (a) Focused image acquired with white light illumination from the projector. (b) Subsurface scattering component image calculated through projection of the high-frequency patterned light. The output value from each RGB channel of the subsurface scattering component image was multiplied by 1.5 and then displayed for easy visual confirmation. (c) Surface reflection component image calculated through projection of the high-frequency patterned light. (d) Diffuse reflection component image calculated using the dichromatic reflection model. (e) Specular reflection component image calculated by subtracting the diffuse reflection component in (d) from the surface reflection component in (c). (f) Image including the diffuse reflection component in (d) and the subsurface scattering component in (b). (g) Average shape created from the shapes of four subjects aged in their 60s. Each 3D image was reconstructed from the focused image and the distance information. Only the viewpoint was changed and the image is displayed as a two-dimensional image here. (h) 3D image reconstructed from the focused image and the distance information. Only the color data of subject C's skin was morphed onto the average shape in (g). The light source and its position were not varied – only the viewpoint was changed and the image is displayed as a two-dimensional image here.

evaluation to evaluate the "skin's visual qualities". Therefore, it is expected to be used in various areas of basic research.

Use of a light field camera allows the system to acquire the facial shape information in a single shot. The captured three-dimensional shape information is displayed to observe the facial image from various angles, as shown in our results. With regard to the light reflected from the skin, the subsurface scattering component and the surface reflection component were first separated by irradiating the skin with a high-frequency pattern, and the diffuse reflection component and the specular reflection component were then separated by applying a dichromatic reflection model to the surface reflection component. By verifying the separation accuracy of the optical properties using four materials with different optical characteristics, we confirmed that the separation of the optical properties by the system can be correlated with the subsurface scattering, specular reflection, or diffuse reflection characteristics of each object. In addition, we verified the separation accuracy for the subsurface scattering and the surface reflection components using resin objects in which the amount of compounded white paint to the crystal resin was physically controlled. It was confirmed that the subsurface scattering component measured by our system correlates with the white paint concentration of resin objects.

Our system separates the diffuse and specular reflections using a traditional dichromatic reflection model, but some recent studies have proposed a method that uses the differences between the images from each microlens of a light field camera to separate the specular reflections [29]. In addition, our system separates the subsurface scattering and surface reflectance components using high-frequency illumination, but other methods have been reported that separate the subsurface scattering into shallow scattering and deep scattering components [17, 20]. It would thus be very interesting to compare the results from these different optical separation methodologies with the skin optical property parameters obtained using our system.

This system can measure the skin condition of each subject in a short time with a remarkably small number of images when compared with other methods, making it suitable for use in the future to confirm the effectiveness of a variety of cosmetics and external skin preparations. In future work, we must analyze the relationship between the subsurface scattering, specular reflection, or diffuse reflection components of the skin and skin physiological parameters including the presence of fine lines, the sebum content and the water content to clarify the skin conditions that affect the optical properties of facial skin by obtaining a wide variety of datasets.

Another important research topic will be to determine how each of the optical property parameters obtained using the proposed system affects the perception of texture aspects such as the glossiness, translucency and dullness of the skin. We would like to clarify the relationship between the physical index of the optical properties and the perception of skin texture and thus contribute to the development of skin texture research.

8. CONCLUSION

In this paper, we have developed a measurement system that divides the light that is reflected from facial skin into the subsurface scattering component, the diffuse reflection component and the specular reflection component, while also acquiring the three-dimensional shape of the subject's face. Verification using physically controlled objects showed that the separation of the optical properties by the system correlated with the subsurface scattering, specular reflection, or diffuse reflection characteristics of each object. This system requires a remarkably small number of images when compared with other measurement methods and can measure the optical property parameters of the subject's facial skin within a short time without burdening the subject. Therefore, this system is expected to be applied not only to skin texture research but also to confirmation of the effectiveness of various cosmetics and external skin preparations.

ACKNOWLEDGMENT

We are grateful to Dr. J. B. Thomas for collaboration and advice on sample measurements. We thank David MacDonald, MSc, from Edanz (https://jp.edanz.com/) for editing a draft of this manuscript. This work was funded by Shiseido Co., Ltd.

REFERENCES

1 T. Igarashi, K. Nishino, and S. K. Nayar, *The Appearance of Human Skin: A Survey* (Now Publishers Inc, Boston, 2007).
2 H. W. Jensen, S. R. Marschner, M. Levoy, and P. Hanrahan, "A practical model for subsurface light transport," *Proc. 28th Annu. Conf. Comput. Graphics Interactive Techn.* (ACM, New York, NY, 2001), pp. 511–518.
3 J. Jimenez, V. Sundstedt, and D. Gutierrez, "Screen-space perceptual rendering of human skin," ACM Trans. Appl. Percept. **6**, 1 (2009).
4 J. Jimenez, D. Whelan, V. Sundstedt, and D. Gutierrez, "Real-time realistic skin translucency," IEEE. Comput. Graph. Appl. **30**, 32 (2010).
5 R. R. Anderson and J. A. Parrish, "The optics of human skin," J. Invest. Dermatol. **77**, 13 (1981).
6 P. R. Bargo and N. Kollias, "Measurement of skin texture through polarization imaging," Br. J. Dermatol. **162**, 724 (2010).
7 A. Matsubara, Z. Liang, Y. Sato, and K. Uchikawa, "Analysis of human perception of facial skin radiance by means of image histogram parameters of surface and subsurface reflections from the skin," Skin Res. Technol. **18**, 265 (2012).
8 Z. X. Jiang and J. DeLaCruz, "Appearance benefits of skin moisturization," Skin Res. Technol. **17**, 51 (2011).
9 A. Matsubara, "Skin translucency: what is it and how is it measured?," *Proc. 24th IFSCC Congress* (IFSCC, Osaka), pp. 92–93.
10 A. Ezerskaia, A. Ras, P. Bloemen, S. F. Pereira, H. P. Urbach, and B. Varghese, "High sensitivity optical measurement of skin gloss," Biomed. Opt. Express. **8**, 3981 (2017).
11 M. Haeri, T. Phamduy, N. Cafone, K. Turkileri, and D. Velkov, "Novel digital image analysis using fractal dimension for assessment of skin radiance," Skin Res. Technol. **25**, 564 (2019).
12 S. Tominaga and A. Kimachi, "Polarization imaging for material classification," Opt. Eng. **47**, 123201.1 (2008).
13 Z. Jiang and P. D. Kaplan, "Point-spread imaging for measurement of skin translucency and scattering," Skin Res. Technol. **14**, 293 (2008).

14 T. Weyrich, W. Matusik, H. Pfister, B. Bickel, C. Donner, C. Tu, J. McAndless, J. Lee, A. Ngan, H. W. Jensen, and M. Gross, "Analysis of human faces using a measurement-based skin reflectance model," ACM Trans. Graph. (SIGGRAPH 2006) **25**, 1013 (2006).

15 T. Kuwahara, "Measurement of Skin Translucency," KOGAKU **39**, 524 (2010) [ISSN: 0389-6625] (in Japanese).

16 S. K. Nayar, G. Krishnan, M. D. Grossberg, and R. Raskar, "Fast separation of direct and global components of a scene using high frequency illumination," *Proc. ACM SIGGRAPH* (ACM, New York, NY, 2006), pp. 935–944.

17 T. Mashita, Y. Mukaigawa, and Y. Yagi, "Measuring and modeling of multi-layered subsurface scattering for human skin," *Proc. Int'l. Conf. on Virtual and Mixed Reality* (Springer, Berlin, Heidelberg, 2011), pp. 335–344.

18 H. Kubo, S. Jayasuriya, T. Iwaguchi, T. Funatomi, Y. Mukaigawa, and S. G. Narasimhan, "Programmable non-epipolar indirect light transport: Capture and analysis," IEEE Trans. Vis. Comput. Graph. **4**, 2421 (2019).

19 P. Debevec, T. Hawkins, C. Tchou, H. P. Duiker, W. Sarokin, and M. Sagar, "Acquiring the reflectance field of a human face," *Proc. 27th Annual Conf. on Computer Graphics and Interactive Techniques* (ACM, New York, NY, 2000), pp. 145–156.

20 A. Ghosh, T. Hawkins, P. Peers, S. Frederiksen, and P. Debevec, "Practical modeling and acquisition of layered facial reflectance," *Proc. ACM SIGGRAPH Asia 2008* (ACM, New York, NY, 2008), pp. 1–10.

21 C. Perwass and L. Wietzke, "Single lens 3D-camera with extended depth-of-field," Proc. SPIE **8291**, 829108 (2012).

22 S. Tominaga, S. Nishi, and R. Ohtera, "Measurement and estimation of spectral sensitivity functions for mobile phone cameras," Sensors **21**, 4985 (2021).

23 S. Lin and H. Y. Shum, "Separation of diffuse and specular reflection in color images," *Proc. IEEE Comput. Soc. Conf. on Computer Vision and Pattern Recognition* (IEEE, Piscataway, NY, 2001), pp. 341–346.

24 S. R. Marschner, S. H. Westin, E. P. Lafortune, K. E. Torrance, and D. P. Greenberg, "Image-based BRDF measurement including human skin," *Proc. Eurographics Workshop on Rendering Techniques* (Springer, Vienna, 1999), pp. 131–144.

25 S. A. Shafer, "Using color to separate reflection components," Color Res. Appl. **10**, 210 (1985).

26 T. Higo, D. Miyazaki, and K. Ikeuchi, "Realtime removal of specular reflection component based on dichromatic reflection model," IEICE PRMU **106.230**, 77 (2006).

27 J. B. Thomas, A. Deniel, and J. Y. Hardeberg, "The plastique collection: A set of resin objects for material appearance research," *Proc. XIV Conferenza del Colore* (Gruppo del Colore Associazione Italiana Colore, Milan, Italy, 2018), pp. 12–23.

28 Pébéo website, accessed on the 19/12/ 2017, http://www.pebeo.com/Pebeo/Plus-de-Pebeo/ARCHIVES/Nouvelles-Resines-Gedeo-de-Pebeo.

29 M. V. Tao, J. C. Su, T. C. Wang, J. Malik, and R. Ramamoorthi, "Depth estimation and specular removal for glossy surfaces using point and line consistency with light-field cameras," IEEE Trans. Pattern Anal. Mach. Intell. **38**, 1155 (2015).